RSC Advances

ROYAL SOCIETY OF CHEMISTRY

www.rsc.org/advances

Enhanced visible light and photocatalytic performance of TiO_2 nanotubes by hydrogenation at lower temperature

*Lijuan Han[a], Zheng Ma[a], Zhihe Luo[b], Gang Liu[a], Jiantai Ma[c], Xingcai An[a, *]*

a. Natural Energy Institute, Gansu Academy of Sciences, Lanzhou 730046, People's Republic of China

b. Northwest Yongxin Coatings Company Limited, Lanzhou 730046, People's Republic of China

c. State Key Laboratory of Applied Organic Chemistry, The Key Laboratory of Catalytic Engineering of Gansu Province and Chemical Engineering, Lanzhou University, Lanzhou 730000, People's Republic of China

* Corresponding author: Tel.: +86-931-8386630; E-mail: anxingcai@unido-isec.org

Abstract: Protonated titanate nanotubes were chosen as precursor in hydrogenation process. Owing to the high capacity for molecular hydrogen storage of naotubes, TiO_2 nanotubes can be hydrogenated through thermal treatment under N_2 and H_2 mixed flow at lower temperature. A series of hydrogenated TiO_2 naotubes and nanobelts were synthesized and characterized by XRD, UV-Vis, TEM, EPR and XPS. The results showed that the hydrogenated TiO_2 nanotubes possess tiny and uniform diameters of 8-10 nm and the walls thickness of 2-3 nm, and were mainly anatase. The anatase TiO_2 nanotubes transformed to TiO_2-B nanobelts when the hydrothermal temperature was higher than 150 ℃. The light absorption of hydrogenated TiO_2 nanotubes was expanded to visible light. However, air-TiO_2 and hydrogenated TiO_2 nanobelts only absorbed ultraviolet light. According to XPS and EPR analysis, hydrogenated TiO_2 nanotubes displayed stable core-shell structures, in which the surface was mainly stoichiometric TiO_2 and the core was non-stoichiometric TiO_2 with Ti^{3+} and oxygen vacancies. The adsorption and photocatalytic performance were evaluated by removal rate of phenol. Based on pseudo-first order kinetic model, the degradation rate constant was obtained with the regression analysis. The highest degradation rate constant of hydrogenated TiO_2 nanotubes was 5.2 times higher than air-TiO_2. In comparison, the degradation rate constants of hydrogenated TiO_2 nanobelts were much lower than air-TiO_2. The results showed that the precursor with nanotubes structure can be hydrogenated easily in lower temperature comparing with nanobelts, resulting in the photocatalytic activity of hydrogenated TiO_2 nanotubes enhanced drastically.

Keywords： TiO_2 nanotubes; Photocatalytic properties; Visible light; Hydrogenation

1. Introduction

Titanium dioxide (TiO_2) is regarded as one of the most ideal photocatalysts. It has promising application in many areas, owing to its nontoxicity, excellent chemical stability, low cost [1-2]. However, the band gap (Eg) of

pristine TiO_2 is too wide, which result in that pristine TiO_2 only absorbs the UV light, limited its practical applications. So for, many approaches involved adding nonmetal [3-6] or metal [7-9] have been used to expand the visible light response range and enhance photocatalytic activity of TiO_2. However, the introduction of dopants, acting as charge carrier recombination centers, easily increases the recombination possibility of photo-generated electron-hole pairs, resulting in the photocatalytic performance decline [10].

Hydrogenated black TiO_2 has been proved to enhance visible light absorption, due to the introduction of electronic state band below the conduction band by oxygen vacancy (V_0) or Ti^{3+} doping and the disorder surface of TiO_2 [11-12]. The light absorption of black TiO_2 can even be extended to infrared region [11], which has aroused great interest of researchers. Recently, black TiO_2 through various methods have been reported [11-21], such as high pressure in H_2 atmosphere [11], plasma assisted hydrogenation [13], high temperature in ordinary pressure [12, 14], hydrothermal method [15, 19, 21]. Among these methods, the method of high temperature (>500℃) in ordinary pressure is easy and simple. However, it is difficult to control the crystallite size of TiO_2 and its photoctalytic activity at high temperature. The lower temperature hydrogenation is helpful to control the crystallite size of TiO_2, but the lower temperature generally leads to incomplete hydrogenation of TiO_2. Herein, we have developed a facile method of hydrogenated TiO_2 at lower temperature (400℃) in ordinary pressure. In the method, the tiny and hollow tubular structure protonated titanate was chosen as precursors. Due to the high capacity for molecular hydrogen storage of protonated titanate nanotubes [22-26], it is possible that the protonated titanate nanotubes are in the hydrogen-rich environment at hydrogenation procedure. The hydrogen-rich environment of nanotubes could reduce the hydrogenated temperature of TiO_2 in ordinary pressure, resulting in that the hydrogenated TiO_2 was generated easily at lower temperature (400℃) under ordinary pressure compared with nanoparticles or nanobelts.

The research results show that the protonated titanate nanotubes were hydrogenated at lower temperature (400℃) in ordinary pressure. And, the protonated titanate nanotubes transformed to black hydrogenated anatase TiO_2 nanotubes in hydrogenation process, which exhibit good visible light response and photocatalytic performance.

2. Experimental section

2.1. Photocatalyst preparation

All chemicals were of analytical grade and used without further purification. TiO_2 precursors (protonated titanate) were prepared by alkaline hydrothermal method and ion exchange [22]. Briefly, a certain amount of

anatase titania powder prepared according to sol-gel method [27] were mixed with 60 mL of 10 mol/L NaOH solution in a Teflon-lined autoclave at appropriate temperature for 24 hours. The hydrothermal temperature affects significantly the morphology and crystal form of material [22-26]. When the hydrothermal temperature is too high, the nanotubes structure of material would transform to nanobelts or nanorods [22, 25]. So, we controlled the tubular shape of material carefully by hydrothermal temperature. The precipitate obtained after alkaline hydrothermal treatment was washed firstly with deionized water until the pH reached about 7, and then immersed in 0.1 mol/L HCl solution overnight with the ion exchange. After that, the precipitate was washed by deionized water again until the pH was about 7 and dried in 100 ℃ for 10 hours. The dried powder was calcinated at 400 ℃ for 4 hours in N_2 and H_2 mixed flow. After that, the sample was cooled fast in inert environment. Finally, the black TiO_2 obtained. The samples prepared at 110 ℃, 130 ℃, 150 ℃, 170 ℃, 190 ℃, 210 ℃ were marked as H-TiO_2(110), H-TiO_2(130), H-TiO_2(150), H-TiO_2(170), H-TiO_2(190), H-TiO_2(210) respectively. Protonated titanate prepared at 130℃ was calcinated at 400 ℃ for 4 hours in air atmosphere to produce TiO_2 without hydrogenation, which was used as reference sample and marked as air- TiO_2.

2.2. Characterizations

The crystal phases of the samples prepared were characterized by the X-ray diffraction (XRD) (D/Max-2400 powder diffractometer) with Cu Kα X-ray source (λ=0.154056 nm) at room temperature. The morphology of the sample was observed on a JEM-2100 transmission electron microscopy (TEM) with an accelerating voltage of 200kV. The chemical states of the samples were characterized by ESCALAB210 X-ray photoelectron spectroscopy (XPS) with an Mg Kα X-ray source. UV-vis spectra of the samples were obtained by UV-vis spectrophotometer (UV-2550) to know ultraviolet and visible light absorption from 200 nm to 800 nm. Electron paramagnetic resonance (EPR) spectra were recorded on a Bruker EMX-10/12 spectrometer at room temperature.

2.3. Adsorption and Photocatalytic Performance Measurement

The adsorption and photocatalytic performance of samples were measured as follow procedure. Herein, phenol was selected as a model pollutant to evaluate the adsorption and photocatalytic activity in visible light. The visible light source was a 300W Xe lamp (Beijing Bofeilai Co., Ltd, Microsolar300) equipped with an AM 1.5 glass filter and a UV-cut-420 nm optical filter. Firstly, 50 mg photocatalyst was dispersed in 250 mL of 10 mg/L aqueous solution of phenol in cylindrical quartz vessel. Then, the suspension above was magnetically stirred in the dark for 30 minutes to reach adsorption−desorption equilibrium. Then, 5 mL dispersion was

withdrawn and centrifuged to test the adsorption activity according to the concentration of phenol. After the adsorption reached equilibrium, the suspension was illuminated by Xe lamp. At 1 hour intervals, 5 mL suspension was withdrawn, centrifuged, and filtered by a 0.22 μm membrane filter to remove the remaining particles. The concentration of phenol at different time interval was measured at λ= 270 nm by UV2500 spectrophotometer (Shimadzu Corporation). Three replicate experiments were performed for every sample.

According to the former works [28-30], the photocatalytic degradation kinetics of phenol can be described using a pseudo-first order kinetic model based on the concentration of phenol:

$$\ln\frac{C}{C_0} = k_p \times t \qquad (1)$$

Where C is the concentration of phenol at t time ($mg.L^{-1}$), C_0 is the initial concentration of phenol, k_p is the apparent first-order reaction rate constant (h^{-1}) determined by regression of experimental data points.

3. Results and discussion

3.1. Structure and morphology characterization

The crystal structure of hydrogenated TiO_2 prepared at different hydrothermal temperatures (110-210℃) and air-TiO_2 were analyzed by XRD, as shown in Fig.1. From Fig.1, it can be seen that hydrothermal temperature significantly influences the formation of crystal structure. When the hydrothermal temperature was from 110 ℃ to 150 ℃, hydrogenated TiO_2 exhibited the phase of pure anatase [16]. Comparing with air-TiO_2, the diffraction peaks of hydrogenated TiO_2 had not obvious shift, and the intensity of hydrogenated TiO_2 became weaker, which is accordance with the other hydrogenation TiO_2 [11, 31].The decrement of the peak intensity can be ascribed to the increase of defect density in the crystal structure. However, when the hydrothermal temperature was higher than 170 ℃, several new broad peaks at 2θ=14.0°, 24.7°, 28.8°, 44.7° appeared, which were in accordance with the patterns of TiO_2-B [32-34]. This means that the anatase had not transformed to rutile but transformed to TiO_2-B at higher hydrothermal temperature.

In order to further probe the morphology of hydrogenated TiO_2 prepared at different hydrothermal temperatures, transmission electron microscopy (TEM) images were obtained, as shown in Fig.2. Fig.2a is the TEM micrograph of hydrogenated TiO_2 prepared at 110 ℃. It shows that most of the material is tubular structure, but a few nanosheets still exist. When the hydrothermal temperature was increased to 130 ℃, it can be seen clearly from Fig.2b that the nanotubes with a nearly uniform diameters (8-10 nm) are dispersed homogeneously, and the lengths of these nanotubes are 50 nm ~ 300 nm. The inset in Fig.2b displays the electron diffraction pattern of these nanotubes. Two diffraction rings in inset is clear, which can be identified as

(200) and (101) of the anatase TiO_2 crystal. The other strong diffractions of anatase TiO_2 crystal are barely identified, which indicates that the shells should consist of a quasi-two-dimensional lattice [24]. Fig.2c is the TEM micrograph of H-TiO_2 (130) at high magnification. The right inset in Fig.2c is an enlarged picture of the nanotube walls as marked by the white circle. Through measurement, the lattice fringes spacing are of around 0.19 nm, corresponding to the (200) plane of the anatase phase, which implied that the axis of TiO_2 nanotubes grew along (200) plane of the anatase phase. With the hydrothermal temperature increased to 150 ℃, these nanotubes (Fig.2d) grew longer and were intertwined each other. It is possible that the long intertwined nanotubes may not store enough molecular hydrogen. Fig.2e is the TEM micrograph of H-TiO_2 (170), which reveals the sample prepared at 170 ℃ is the mixture of nanobelts and naotubes. When the hydrothermal temperature was increased to 210 ℃, the naotubes had entirely transformed to TiO_2 nanobelts. From Fig.2f, it can be seen that the width of TiO_2 nanobelts was about 50 nm and many TiO_2 nanobelts overlapped each other. The inset in Fig.2f displays the electron diffraction pattern of these nanobelts. The electron diffraction pattern is accordance with the other report about TiO_2-B [32, 34], which implied that the crystal phase had changed to TiO_2-B at higher hydrothermal temperature. The result is consistent with analysis of XRD.

The UV-visible diffuse reflectance spectra of hydrogenated TiO_2 nanotubes prepared in different hydrothermal temperatures and air-TiO_2 are shown in Fig.3. It can be seen that air-TiO_2 only responds to ultraviolet light. The hydrogenated TiO_2 nanotubes (H-TiO_2(110), H-TiO_2(130), H-TiO_2(150)) had absorption tail in the visible light regions. And, the onset of the optical absorption of hydrogenated TiO_2 nanotubes had not exhibited red shift comparing with air-TiO_2, which implies the valence band or conduction band had not shift. As reported previously [26], V_0 and Ti^{3+} in hydrogenated TiO_2 nanotubes would be formed as isolated states in the band gap of TiO_2 to induce visible light absorption, rather than a shift in the position of either band edges. However, the light response of hydrogenated TiO_2 (H-TiO_2(170), H-TiO_2(190), H-TiO_2(210)) had not been expanded to visible light but had a shift to ultraviolet light, which may be due to band structure of TiO_2-B itself on the one hand, on the other hand, the nanobelts possess low capacity for molecular hydrogen storage, resulting in incomplete hydrogenation. So, the visible light response of these samples (H-TiO_2(170), H-TiO_2(190), H-TiO_2(210)) are lower obviously than hydrogenated TiO_2 nanotubes (H-TiO_2(110), H-TiO_2(130), H-TiO_2(150)), even air-TiO_2.

To further examine the effect of hydrogenation on the chemical composition of TiO_2 nanotubes surfaces, XPS spectra of the hydrogenated TiO_2 nanotubes prepared in 130 ℃ and air-TiO_2 were investigated. In order to

avoid the effect of carbon caused in hydrogenation, the samples were sputtered by Au before measurement. Fig. 4(a) presents the Ti 2p XPS spectra of air-TiO_2 and H-TiO_2 (130). From Fig.4(a), it can be seen that both of H-TiO_2(130) and air- TiO_2 had two symmetric peaks at ~464.6, ~458.8 eV, respectively, which are the characteristic Ti $2p_{1/2}$ and Ti $2p_{3/2}$ peaks of Ti^{4+} [16, 19, 25]. The Ti 2p XPS spectrum of hydrogenated TiO_2 nanotubes did not give any Ti^{3+} or Ti^{2+} signals , which indicated that no titanium with lower oxidation states were detected in the surface of samples. So, we deduce that the surface of hydrogenated TiO_2 nanotubes is made of stoichiometric TiO_2.

Since Ti^{3+} was not detected by XPS analysis, EPR of hydrogenated TiO_2 nanotubes (H-TiO_2(110) H-TiO_2(130), H-TiO_2(150), H-TiO_2(170)) and air-TiO_2 were conducted to further identify the presence of oxygen vacancy and Ti^{3+}. The EPR spectra are shown in Fig.4(b). According to Fig.4(b), all the hydrogenated TiO_2 samples gave rise to a signal at $g = 2.002$, which is the typical g value for paramagnetic Ti^{3+} centers due to the oxygen depletion [35,36]. However, the hydrogenated TiO_2 samples revealed the different intensity, which implied the different Ti^{3+} concentration. The EPR intensity of hydrogenated TiO_2 nanotubes, such as H-TiO_2(110), H-TiO_2(130) and H-TiO_2(150), were very strong. The intensity of hydrogenated TiO_2 nanobelts (H-TiO_2(170)) was lower than the others, which implied the low concentration of Ti^{3+} of hydrogenated TiO_2 nanobelts and the high concentration of Ti^{3+} of hydrogenated TiO_2 nanotubes. Because the concentration of Ti^{3+} is related to the degree of hydrogenation, the different concentrations of Ti^{3+} of hydrogenated TiO_2 imply that the nanotubes are easily hydrogenated than nanobelts, which is accordance with our speculation. As reported, when a part of Ti^{3+} located in the surface of TiO_2 nanotubes, the surface Ti^{3+} can efficiently trap oxygen molecules on defect sites to form $\bullet O_2^-$, which can generate another EPR signal. This signal has not been found in all the EPR spectra, which imply that Ti^{3+} is absent from the surface of the hydrogenated TiO_2. The result is in good agreement with XPS analysis. In contrast, air-TiO_2 had not shown any signals at the same measurement condition, which reveals that there was not any Ti^{3+} in the bulk or the surface for air-TiO_2. EPR result reveals that a high concentration of Ti^{3+} was located in the bulk of TiO_2 nanotubes, resulting in defective and non-stoichiometric TiO_2. In addition, the surface of hydrogenated TiO_2 nanotubes is composed of stoichiometric TiO_2. The stable stoichiometric TiO_2 can protect Ti^{3+} in the bulk of TiO_2 nanotubes from being oxidized while non-stoichiometric TiO_2 in the bulk promote visible light response and photocatalytic activity. The structure is similar to the core-shell structure of hydrogenated TiO_2 nanoparticles prepared by the other methods [12, 37], which is considered stable and high photocatalytic activity.

3.2 Adsorption and photocatalytic performance of the samples

The relative concentrations plotted over time for the adsorption and photocatalytic performance of as-prepared samples are presented in Fig.5. The result shows that all samples have scarcely any adsorption activity for phenol. So, the effect of adsorption activities of samples compared with their photocatalytic performance can be ignored. For the photocatalytic performance of the samples, phenol can be degraded in different extent under visible light irradiation. Among these samples, the hydrogenated TiO_2 nanotubes prepared at 110℃, 130℃, 150℃ exhibited high photocatalytic activity for phenol. However, the hydrogenated TiO_2 prepared at 170℃, 190℃, 210℃ exhibited very poor photocatalytic activity for phenol, even badly than air-TiO_2.

The photocatalytic degradation of phenol follows an apparent first-order reaction. Based on pseudo-first order kinetic model (Eq. (1)) [28-30], the degradation rate constant (k_p) is obtained with the regression analysis based on the minimization of the squared errors, and the correlation coefficient of the line is also presented (R^2). The results of the regression analysis for these samples are given in Table 1. It is known that an R^2 closer to 1.0 indicates that the regression line perfectly fits the data [29]. From Table 1, it can be seen that the R^2 values of the most of samples were higher than 0.96, and only the R^2 values of H-TiO_2(190) and H-TiO_2(210) were about 0.94, which mean the regression analysis is credible.

In order to probe whether the hydrogenation is beneficial to the photocatalytic performance of TiO_2 or not, the degradation rate constants of the samples are compared, as shown in Fig.6. It is obviously that the hydrogenation has not always enhanced the photocatalytic performance. When the structure of TiO_2 is nanotubes (hydrothermal temperature ≤ 150℃), all the degradation rate constants of hydrogenated TiO_2 nanotubes are much higher than air-TiO_2. The highest degradation rate constant of hydrogenated TiO_2 nanotubes (H-TiO_2(130)) reaches to 0.1559 h^{-1}, which is 5.2 times higher than air-TiO_2. Furthermore, the degradation rate constant of hydrogenated TiO_2 nanotubes (H-TiO_2(150)), which is the lowest among the hydrogenated TiO_2 nanotubes, is higher than air-TiO_2. However, when the structure of TiO_2 is nanobelts (hydrothermal temperature ≥ 170℃), the degradation rate constants are lower than air-TiO_2. It shows that the structure of precursor and crystal phase effect significantly the photocatalytic performance. The hydrogenated anatase TiO_2 nanotubes with high concentration of oxygen vacancies and Ti^{3+} exhibit high photocatalytic activity while the hydrogenated TiO_2-B nanobelts exhibit low photocatalytic activity.

The high concentration of oxygen vacancy and Ti^{3+} species presented in hydrogenated anatase TiO_2

nanotubes would form some isolate defect energy levels in the band gap, which not only enhance the visible light absorption of photocatalysts but also suppress the recombination of electron-hole pairs to promote the photocatalytic activity. In contrast, the concentration of oxygen vacancies and Ti^{3+} of hydrogenated TiO_2-B nanobelts is lower than hydrogenated anatase TiO_2 nanotubes, which may not enough to increase the photocatalytic performance. More importantly, the photocatalytic activity of TiO_2-B crystal is usually lower than anatase crystal, caused the poor photocatalytic performance of hydrogenated TiO_2-B nanobelts.

Among the photocatalysts of (H-TiO_2(110), H-TiO_2(130), H-TiO_2(150), H-TiO_2(130) had the highest photocatalytic activity, and its removal rate for phenol was about 4 times of air-TiO_2 after 6 hours illumination. Compared with H-TiO_2 (110), H-TiO_2 (150), H-TiO_2 (130) is composed of the short and thin nanotubes which can adsorb a large number of molecular hydrogen causing the most effective hydrogenation. Owing to the effective hydrogenation, more oxygen vacancies and Ti^{3+} were generated, which is confirmed by EPR data. So, the visible light photocatalytic activity of H-TiO_2 (130) was the best due to the higher visible light response and electron-hole separation efficiency.

3.3 The mechanisms of formation of hydrogenated nanotubes

The mechanism of hydrogenated nanotubes was illustrated by Fig.7. Owing to the protonated titanate nanotubes possess a high capacity for molecular hydrogen storage and many protons on their walls [14], the walls of protonated titanate nanotubes adsorb a large number of hydrogen molecules. According to TEM analysis, TiO_2 nanotubes grow along (200) plane of the anatase phase. The (200) plane of nanotube is exposed with mainly unsaturated O and Ti modes. These molecular hydrogens are easily adsorbed on the unsaturated O and Ti sites favorably under the H_2 atmosphere [14, 38]. With the temperature increasing(Ⅰ), OH bands are formed in the first stage of annealing on the surface of TiO_2 nanotubes. Meanwhile, it is possible that Ti-H bonds on the surface of nanotubes are formed, which make the surface Ti recovered octahedral coordination. Upon increasing the annealing temperature(Ⅱ), Ti-OH and Ti-H become unstable and produced H_2O molecules, which result in formation of more oxygen vacancies [39]. With the formation of oxygen vacancies (V_o), low valence titanium (Ti^{3+}), are formed. Furthermore, hydrogen molecules pass into the bulk of TiO_2 nanotubes forming more V_o and Ti^{3+} in its lattice. Then, through fast cooling in inert environment, the active surface is freezed and V_o and Ti^{3+} in its lattice are protected [12]. Oxygen vacancy and Ti^{3+} form located states between conduction band and valence band, which can enhance the efficiency separation of the photogenerated electron-hole and extend the visible light absorption. And then, the photocatalytic activity of hydrogenated

TiO_2 nanotubes in visible light was enhanced remarkably.

4. Conclusions

In summary, nanotubles and nanobelts protonated titanate were prepared by alkaline hydrothermal method. Through calcinating protonated titanate in N_2 and H_2 mixed flow at lower temperature (400℃), hydrogenated nanotubles anatase and hydrogenated nanobelts TiO_2-B obtained. Hydrogenated nanotubles have stable core-shell structure and exhibit excellent photocatalytic activity while hydrogenated nanobelts TiO_2-B exhibit poor photocatalytic activity. Due to high capacity for molecular hydrogen storage of nanotubes, the protonated titanate nanotubes can be easily hydrogenated at mild condition. With the effective hydrogenation, oxygen vacancies and Ti^{3+} were generated, which not only enhance the separation efficiency of the photogenerated electron-hole but also extend the visible light absorption. The highest degradation rate constant of hydrogenated TiO_2 nanotubes in visible light is 5.2 times higher than air-TiO_2. It reveals that the photocatalytic activity of hydrogenated TiO_2 nanotubes in visible light was enhanced remarkably.

Acknowledgements

The authors are grateful for financial aid from Key Science and Technology Foundation of Gansu Province (143GKDA013), Youth Science and Technology Fund of Gansu Province (1308RJYA051), and Youth Science and Technology Innovation Fund of Gansu Academy of Sciences (2013QN-16).

References

[1] Venkatachalam N.; Palanichamy M.; Murugesan V. *Mate.Chem.Phys.* **2007**, 104, 454-459.

[2] Hussain M.; Ceccarelli R.; Marchisio D.; Fino D.; Russo N.; Geobaldo F. *Chem.Eng. J.* **2010,** 157, 45-51.

[3] Asahi R.; Morikawa T.; Ohwaki T.; Aoki K.; Taga Y. *Science.* **2001**, 293, 269-271.

[4] Ananpattarachai J.; Kajitvichyanukul P.; Seraphin S. *J.Hazard.Mater.* **2009**, 168, 253-261.

[5] Liu S.; Chen X. *J.Hazard.Mater.* **2008**, 152, 48-55.

[6] Li H.; Wang D.; Fan H.; Wang P.; Jiang T.; Xie T. *J.Colloid.Interface. Sci.* **2011**, 354,175-180.

[7] Jeffrey C;Chen C. *J. Photoch. Photobio. A: Chem.* **2004**, 163,509–515.

[8] Lazau C.; Sfirloaga P.;Orha C.; Ratiu C.; Grozescu L. *Mater. Lett.* **2011**, 65, 337-339.

[9] Liu J.; Han R.; Zhao Y.; Wang H.; Lu W.; Yu T.; Zhang Y. *J. Phys.Chem.C.* **2011**, 115, 4507-4515.

[10] Tan K.; Zhang H.; Xie C.; Zheng H.; Gu Y.; Zhang W. *Cataly. Commun.* **2010**, 11,331-335.

[11] Chen X.; Liu L.; Yu P.; Mao S. *Science* .**2011**, 331, 746-750.

[12] Naldoni A.;Allieta M.; Santangelo S.; Marelli M,; Fabbri F.; Cappelli S.; Bianchi C.; Psaro R.; Santo V. *J. Amer. Chem. Soc.* **2012**, 134,7600-7603.

[13] Pranevicius L.; Milcius D.;Tuckkute S.; Gedvilas K. *Appl. Surf. Sci.* **2012**, 258, 8619-8622.

[14] Zheng Z.; Huang B. Lu J.; Wang Z,; Qin X.; Zhang X.; Dai Y.; Whanqbo M. *Chem. Commun.* **2012**, 48,5733-5735.

[15] Zhao Z,; Tan H.; Zhao H.; Lv Y.; Zhou L.; Song Y.; Sun Z. Chem.Commun. 2014,50,2755-2757.

[16] Xia T.; Chen X. *J.Mater. Chem. A.* **2013**, 1, 2983-2989.

[17] Leshuk T.; Parviz R.; Everett P.; Krishnakumar H.; Varin R.; Gu F. *Appl.Mater.Interfaces.* **2013**, 5, 1892-1895.

[18] Zheng Z.; Huang B.; Meng X.; Wang J.; Wang S.; Lou Z.; Wang Z.; Qin X.; Zhang X.; Dai Y.*Chem. Commun.* **2013**, 49, 868-870.

[19] Liu X.; Gao S.; Xu H.; Lou Z.; Wang W.; Huang B.; Dai Y.*Nanoscale.* **2013**, 5, 1870-1875.

[20] Tan H.; Zhao Z.; Niu M.; Mao C.; Cao D.; Cheng D.; Feng P.; Sun Z. *Nanoscale.* **2014**, 6, 10216-10223.

[21] Wang W.; Ni Y.; Lu C.; Xu Z.RSC Advances,2012,2,8286-8288

[22] Zhao B.; Chen F.; Jiao Y.; Zhang J. *J.Mater.Chem.* **2010**,20,7990-7997.

[23] Wang Y.; Hu G.;Duan X.;Sun H.;Xue Q. *Chem.Phys.Lett.***2002**,365,427-431.

[24] Yao B.; Chan Y.; Zhang X.; Zhang W.; Yang Z.; Wang N. *Appl.Phys. Lett.* **2003**,82,281-283.

[25] Liu W.;Gao J.;Zhang F.;Zhang G. *Mater.Trans*.**2007**,48,2464-2466.

[26] Putdee S.;Mekasuwandumrong O.; Soottitantawat A.;Panpranot J. *Ceram. Int.* **2014**,40,2323-2329.

[27] An X.; Han L.; Chen Z.; Liu G.;Xi W. *Acta Energiae Solaris Sinica.* **2012**,33,874-877.

[28] Van Doorslaer, X.; Demeestere, K.; Heynderickx, P. M.; Van Langenhove, H.; Dewulf. *App.Catal. B-Environ.* **2011**, 101(3), 540-547.

[29] Huang, X.; Feng, Y.; Hu, C.; Xiao, X.; Yu, D.; Zou, X. *Chemosphere*. **2015**,138, 183-189.

[30] Abdullah, M. A.; Chong, F. K. Chem. Eng. J. **2010**, 158(3), 418-425.

[31] Wang G.; Wang H.; Ling Y.; Tang Y.; Yang X.; Fitzmorris R.; Wang C.; Zhang J.; Li Y. *Nano Letter*.**2011**,11,3026-3033.

[32] Pavasupree S.; Suzuki Y.;Yoshikawa S.; Kawhata R. *J. Solid. State. Chem.***2005**,178,3110-3116.

[33] Suzuki Y.; Pavasupree S.; Yoshikawa S.; Kawhata R. *J.Mater Res.***2005**,20,1063-1070.

[34] Zhao B.; Chen F.; Qu W.; Zhang J. *J. Solid. State. Chem.***2009**,182,2225-2230.

[35] Huo, J.; Hu, Y.; Jiang, H.; Li, C. *Nanoscale*. **2014**, 6(15), 9078-9084.

[36] Napoli, F.; Chiesa, M.; Livraghi, S.; Giamello, E.; Agnoli, S.; Granozzi, G.; Di Valentin, C. *Chem. Phys.*

Lett. **2009**, 477(1), 135-138.

[37] Zhu Q.; Peng Y.;Lin L.; Fan C.; Gao G.; Wang R.; Xu A. *J. Mater. Chem. A*. **2014**, 2, 4429-4437.

[38] Tian F.; Zhang Y.; Zhang J.; Pan C. *J. Phys. Chem.C.* **2012**,116,7515-7519.

[39] Wang W.; Lu C.; Ni Y.; Su M.; Xu Z. *App.Catal. B-Environ.* **2012**, 127, 28-35.

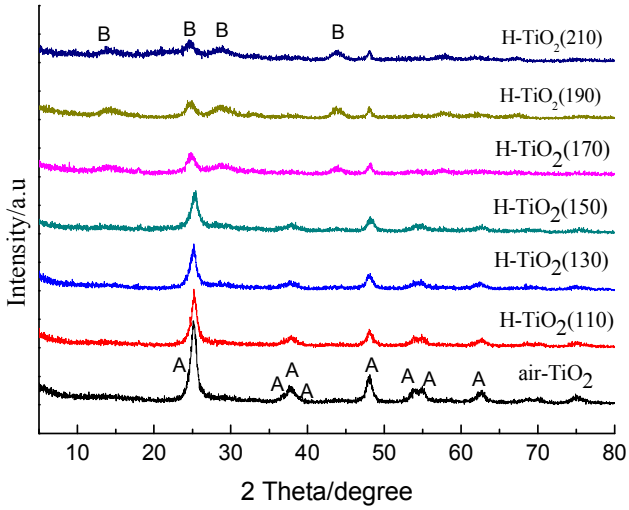

Fig. 1. XRD patterns of H-TiO_2(110), H-TiO_2(130), H-TiO_2(150), H-TiO_2(170), H-TiO_2(190), H-TiO_2(210) and air-TiO_2; A: anatase TiO_2, B: TiO_2-B

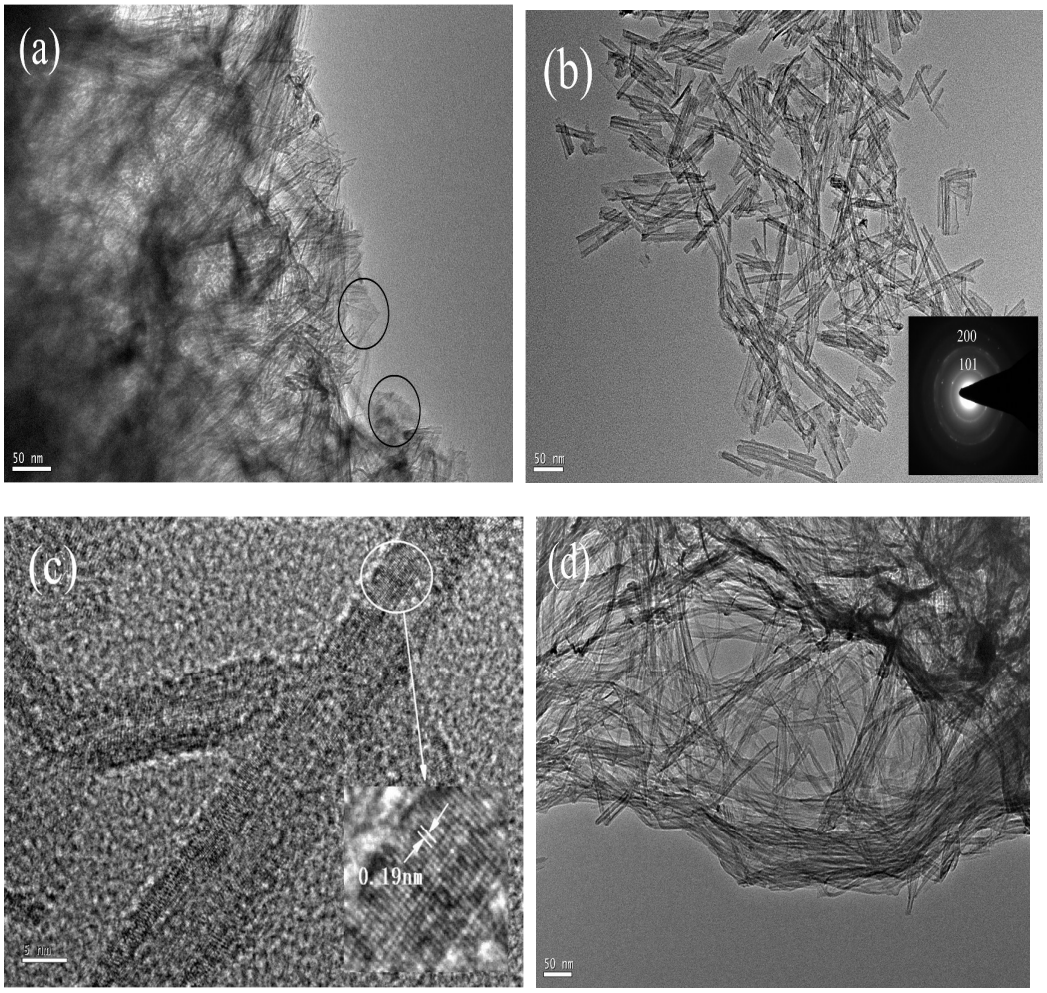

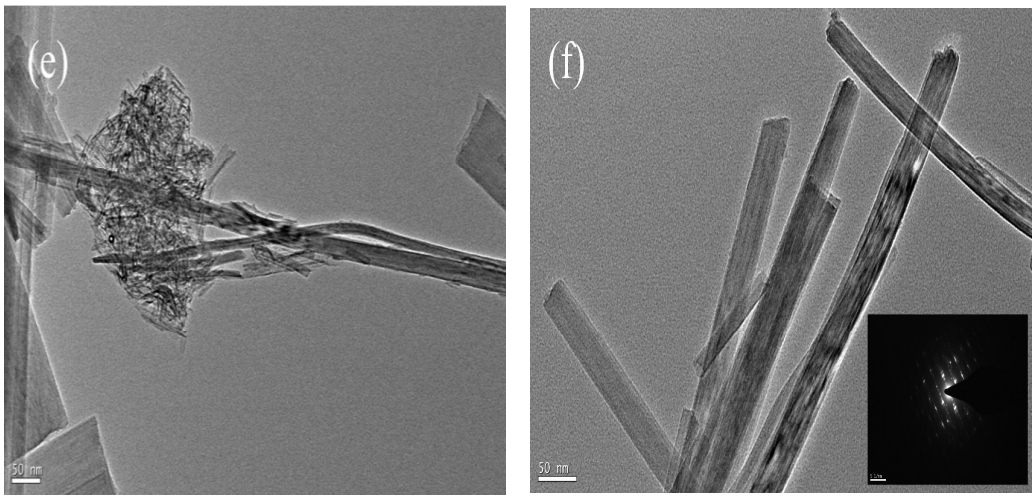

Fig. 2. TEM images of hydrogenated TiO_2 (a: TEM image of H-TiO_2 (110); b: TEM image of H-TiO_2 (130) at low magnification, the inset is electron diffraction pattern; c: TEM image of H-TiO_2 (130) at high magnification, the inset is the enlarged picture of nanotube wall; d: TEM image of H-TiO_2 (150); e: TEM image of H-TiO_2 (170); f: TEM image of H-TiO_2 (210), the inset is electron diffraction pattern.

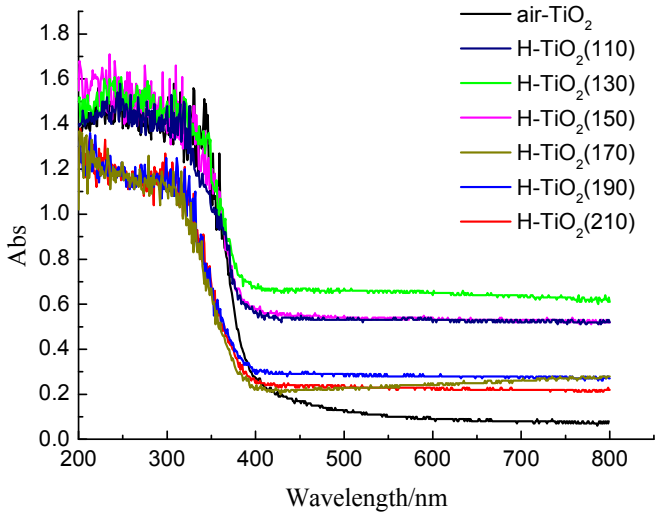

Fig.3. UV- visible diffuse reflectance spectra of H-TiO_2(110), H-TiO_2(130), H-TiO_2(150), H-TiO_2(170), H-TiO_2(190), H-TiO_2(210) and air-TiO_2

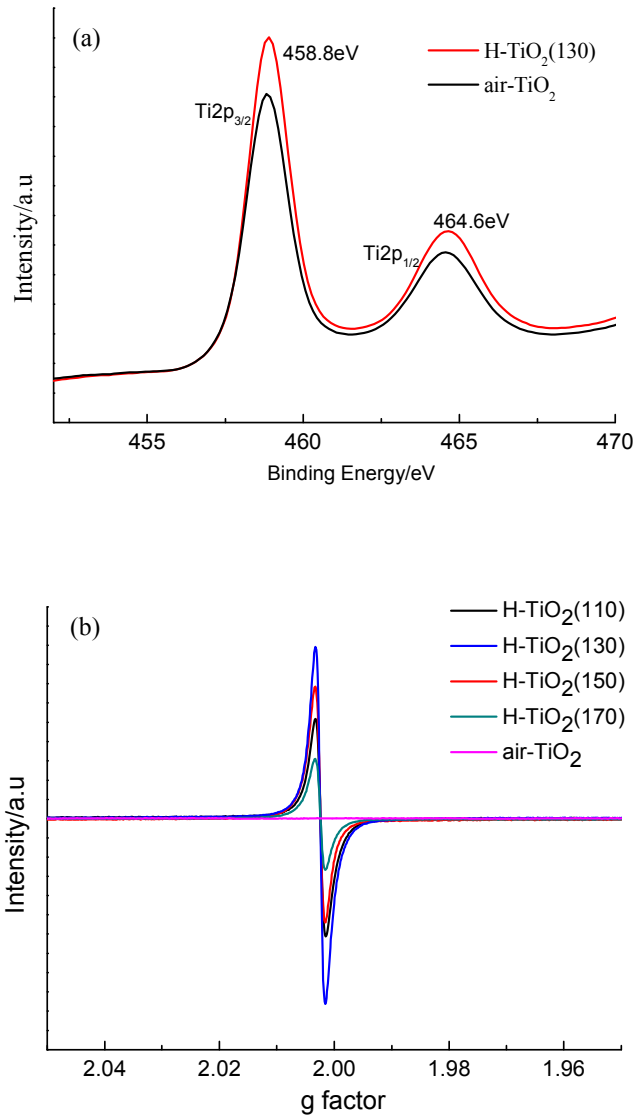

Fig .4. (a) XPS spectra of hydrogenated TiO_2 nanotubes(H-TiO_2(130) and TiO_2 without hydrogenation(air-TiO_2). (b) EPR spectra of H-TiO_2(110), H-TiO_2(130), H-TiO_2(150), H-TiO_2(170), and air-TiO_2

.

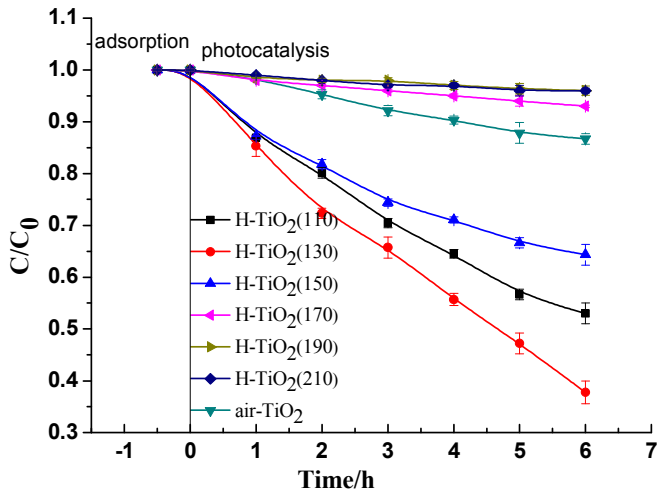

Fig. 5. Adsorption and photocatalytic performance for degradation phenol of H-TiO_2(110), H-TiO_2(130), H-TiO_2(150) , H-TiO_2(170), H-TiO_2(190), H-TiO_2(210) and air-TiO_2

Table 1

Samples	k_p	R^2
H-TiO_2(110)	0.1036 ± 0.002	0.9947
H-TiO_2(130)	0.1559 ± 0.005	0.9918
H-TiO_2(150)	0.0715 ± 0.003	0.9654
H-TiO_2(170)	0.0115 ± 0.001	0.9869
H-TiO_2(190)	0.0069 ± 0.001	0.9418
H-TiO_2(210)	0.0063 ± 0.001	0.9469
air-TiO_2	0.0253 ± 0.002	0.9896

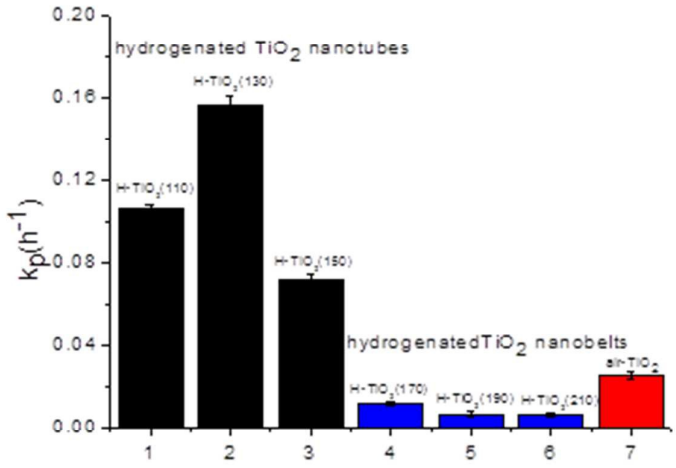

Fig. 6. Apparent firs-order degradation constants k_p (h^{-1}) for photocatalysis of H-TiO_2(110), H-TiO_2(130), H-TiO_2(150) , H-TiO_2(170), H-TiO_2(190), H-TiO_2(210) and air-TiO_2

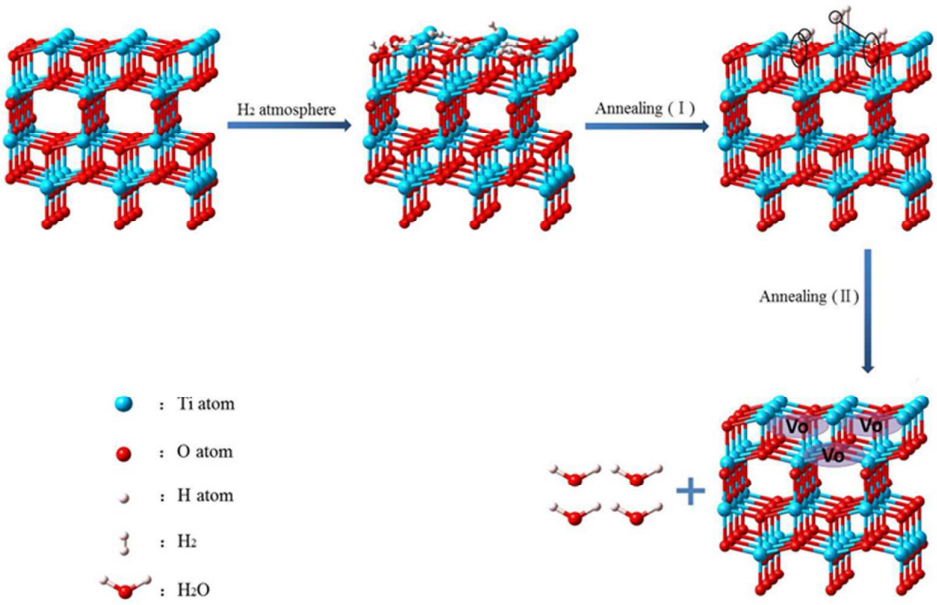

Fig. 7. Schematic illustration of the formation process of hydrogenated nanotubes